Impact of external static electric field on surface tension of model solutions

Adrien Garcia, Tzvetelin Dessev, Luc Guihard, Sylvie Swyngedau Chevallier, Michel Havet, Alain Le-Bail

Impact of external static electric field on surface tension of model solutions

Adrien Garcia[(1)], Tzvetelin Dessev[(2)], Luc Guihard[(1)], Sylvie Swyngedau Chevallier[(1)], Michel Havet[(1,a)], Alain Le-Bail[(1)]

(1) ONIRIS, Nantes Université, CNRS, GEPEA, UMR 6144, Nantes, F-44000, France
(2) Nofima Mat, Food and Health Department, As 1430, Norway
(a) michel.havet@oniris-nantes.fr

HIGHLIGHTS

- Tensiometer measures liquid droplets surface tension under electric field.
- 3 model solutions used: water, WPI solution, and chickpea aquafaba.
- For protein solutions, significant reduction of surface tension was determined.

KEYWORDS

Surface tension reduction, static electric field, pendant droplet tensiometer, Laplace equations, image analysis

ABSTRACT

Food foams are thermodynamically unstable systems. Their stabilization remains a challenge in the industry. To understand the interactions between an electrostatic field (SEF) and food foam, a microscopic study was conducted. Using a specially designed tensiometer, a liquid droplet (water, WPI solution, chickpea liquor) was placed between two parallel electrodes and subjected to an SEF (0 to 800 kV/m). Images of the pendant droplet were recorded throughout the experiment. Based on Laplace's equation, the surface tension was calculated as function of the applied voltage.

The geometry of the droplet was deformed under SEF. The surface tension decreased proportionally to the rise of the voltage ($\gamma_{distilled\ water} = 21.7.10^{-3}$ N/m at 800 kV/m).

The mechanism causing surface tension reduction was found to be the electric charge existing on the liquid surface. By reducing surface tension, drops are likely to break up more easily during expansion, which improves the organoleptic qualities of the foam.

1. INTRODUCTION

Aerated products represent a major part of the products processed by the food industry. They can be found in almost all kinds of food categories in a wide variety of forms: bread, beer foam, dessert foams, ice cream, etc. A food foam is defined as a biphasic structure in which one of the two phases, the gas in this case, is dispersed in variable diameter bubbles in a continuous phase which may be liquid, semi-solid or solid (Talansier et al., 2012).

Although food foams are now widely available, their production, and especially their stabilisation over time, remains a challenge for manufacturers. Foams are thermodynamically unstable objects. The smaller gas bubbles in the continuous phase will naturally seek to merge with each other to form larger bubbles in order to lower their internal pressure (Schramm 2006). The liquid phase will tend to separate from the gas phase by migrating downwards in the product, under the effect of gravity (Audebert 2018; Boissonnet 1998). The destabilization mechanisms are numerous but they are all linked to the same phenomenon, namely an excess of surface tension at the gas/liquid interfaces.

The "surface tension" (ST) is linked to an attractive intermolecular force associated to the cohesion of the molecules. In terms of energy, the surface tension can be seen as the energy required per unit area to create an interface between two immiscible materials - fluids or solids. According to Castellanos (1998), an increase in surface area ΔA requires work W such that:

$$W = \sigma . \Delta A \quad (1)$$

- with σ, surface tension (N.m-1)

Numerous studies demonstrated the importance of lowering ST to promote foam expansion (Nicorescu 2009). Today, manufacturers use energy-intensive mixers to generate foams with small bubbles; the use of surfactants is often considered to lower the surface tension. However, extrapolating the work done on dielectric materials to food matrices, foam generation, coupled with the use of a static electric field (SEF), appears to be an innovative method that would enable to durably stabilize a foam, by limiting the use of additives in the formulation, while reducing the energy consumption and the viscous dissipation (heatup) during processing.

In the field of thermal processes and heat transfer, Siedel (2012) performed boiling experiments in the presence of 50 $kV.cm^{-1}$ electric fields, and the effect of SEF on heat transfer and bubble dynamics was characterized. The modification of the convective structures by the presence of SEF was described, showing smaller convective cells and more intense convective

activity. The consequent enhancement of heat transfer was quantified showing that the vapour production rate is decreased during bubble growth. The electrohydrodynamic effects on bubble dynamics was investigated showing that the bubble growth curve was modified but there is no clear influence of the SEF concerning the bubble departing frequency and the volume at departure. Although the volume of the bubbles at detachment and the relationship between the bubble frequency and the wall superheat were not affected, the bubble growth curve was modified. Siedel observed that bubbles were elongated in the direction of the SEF. The rising velocity of the bubble was also reduced in the presence of SEF, and the behaviour of bubbles growing side by side was modified, the SEF causing the bubbles to repel each other. These results provide compelling evidence that SEF can alter the bubble dynamics and subsequently heat transfer rates during boiling of dielectric fluids.

By focussing on the atomisation process, Sato et al. (1997) showed that the applied SEF enhanced atomisation because it was responsible for the decrease of the average diameter of formed droplets, due to ST reduction. Reduction of ST due to the applied voltage was proportional to the square of the voltage. The reduction varied with the electrical conductivity of the liquid and when the electrical conductivity > $l0^2$ $S.m^{-1}$, the measured reduction was in good agreement with theory.

However, in the fields of chemical foams, Bonhomme et al. (2020) showed that applying an external SEF at the edge of the foam induces some liquid flows and, depending on the flow magnitude, it controls either gravity driven drainage, the foam stability, or the foam collapse at a specific location. While the liquid fraction of a foam tends to decrease as a function of foam height and time, at certain very specific values of capillary number and SEF, there is a reversal of the trend: the application of an SEF can therefore reverse the drainage.

The dynamics of droplet formation under the influence of an external SEF have been also studied by numerical investigation (Notz and Basaran 1999; Borthakur, Biswas, and Bandyopadhyay 2018). The studies were mostly carried out by solving axisymmetric electrohydrodynamic equations. The studies revealed that under the influence of an SEF, prolate-shaped droplets are formed at the orifice in the case of perfect dielectric fluids. The applied SEF strength and the ratio of the dielectric permittivity of the fluids play a pivotal role in deciding the magnitude of deformation as well as the volume of the droplets. The local SEF intensity inside the droplet is significantly altered due to the permittivity contrast between the fluids. The computations for leaky dielectric fluids reveal that both prolate - and oblate - shaped

droplets can be formed depending on the combination of the fluid conductivity and permittivity ratios (Borthakur, Biswas, and Bandyopadhyay 2018). The breakup time and detached droplet volume can be suitably tuned by varying the strength of the applied SEF.

All these elements suggest that generating a foam under a SEF would have an influence on the gas/liquid interface that constitutes each bubble contained in the foam. If the SEF reduces the surface tension, then the generation of small diameter bubbles would be facilitated with a lower energy consumption with an enhanced thermodynamic stability.

This paper presents the experiments carried out to validate these hypotheses. The authors have chosen to work at the scale of a droplet of liquid, generated with a pendant droplet tensiometer (Felix et al. 2021), from a protein solution, modelling a food matrix. The mechanisms that govern the stability of a foam take place at the gas/liquid interfaces. Therefore, the study of a liquid droplet in a gaseous environment allows a simple study of the mechanisms at the interfaces. While we have worked on liquid droplets for experimental convenience, the observations and results obtained could easily be transposed to gas bubbles (the case of food foams), because the real object of study is the gas/liquid interface. Using Laplace's equation and image analysis, the ST was calculated as a function of the applied tension. The novelty of this work lies in the experimentation on non-insulating matrices, such as food matrices.

2. MATERIAL & METHODS

2.1. Model solutions

To study the impact of the SEF at the scale of a droplet of liquid, three model solutions were selected. Distilled water was first considered as a control solution. Indeed, the value of the surface tension of water at 0 kV is well known in the literature (Kovalchuk, Alberini, and Simmons 2020; Yousif et al. 2021; Liu and Cao 2021): it is 72 $mN.m^{-1}$. The measurement of the ST of a droplet of water was used as a reference measurement in order to compare it to the measurements made with two other model solutions.

The foam-type food matrices can be assimilated to liquid protein solutions in which a gas injection is performed. The second model solution was an aqueous solution of Whey Protein Isolate (WPI). WPI is a protein of animal origin, an isolate's short chain proteins that are extracted from Whey Protein Concentrate also known as WPC, derived from milk. Techno-physical properties such as ST (Bazinet, Trigui, and Ippersiel 2004), viscosity (Bazinet, Trigui, and Ippersiel 2004; Wang et al. 2021) or gas solubility (Said et al. 2022) of WPI-based solutions are available in the literature. This is why we chose to use this first protein solution in order to

reconcile our results with existing data. Several works (Laporte, 2014; Nicorescu, 2009; Talansier et al, 2012) highlighted the difficulty of dissolving WPI in the aqueous phase and obtaining a homogeneous solution. Based on the work of Talansier et al. (2012), we defined a protocol specific to our experiment. We decided to prepare solutions containing 3% WPI. The total mass of WPI was incorporated in 4 times, staggered at 15mn intervals, under moderate agitation (3-blade propeller, speed 100 rpm), at room temperature (20°C), to guarantee the complete dissolution of the powder. After complete dissolution of the WPI, the solution was transferred into the pendant droplet tensiometer.

Considering a clean label approach, a protein of plant origin was considered for the third model solution, namely an aqueous chickpea protein solution (CKP). According to Buhl et al. (2019), aquafaba has shown good food functional properties, as this plant-based liquid has the ability to function as both a foaming agent and an emulsifier under conditions of pH and NaCl concentrations that happen to be those readily encountered in food products. As a vegetable alternative to egg white or WPI, CKP aquafaba seems to be an interesting candidate for foamed products. Therefore, we decided to use a chickpea aquafaba-based solution. The aquafaba from 10 cans was collected by sieving. It was then centrifuged to ensure homogeneity of the mixture. A sample of this aquafaba was taken for determination of the protein content by the Dumas method (protein content of 3% +/- 0.2%).

The distilled water and the WPI and CKP solutions made the 3 model solutions used in this study, which will imitate the behaviour of gas/liquid interfaces of foam-type food matrices in the presence of an SEF.

2.2. Experimental set-up

The liquid droplet was generated using a TRACKER™ automatic droplet tensiometer, manufactured by TECLIS Instruments (formerly IT Concept) and modified to allow a high voltage generator (Figure 1). The droplet had a volume of ca. 8µL, which was regulated by a PID system. Volumetric calibration was performed by the software supplied with the equipment. The observation of the droplet was done with a fast camera (MELLES GRIOT / CCD / 640x480 / 60 frames per seconds) illuminated by a stroboscopic LED light source (180 lm / ø 45mm). Using a high voltage source (Ottersweier), an electric field was applied to the droplet using two parallel electrodes (10x45mm / 1mm thick / stainless steel), positioned on either side of the droplet, in a 3D printed ABS plastic holder (1.25 cm wide square section).

The experiment consisted of applying several positive voltage values: 0 kV ; +0.5 kV ; +1 kV ; +1.5 kV ; +2 kV ; +4 kV ; +6 kV ; +8 kV ; +10 kV. With the geometry of our experimental set up, this corresponds to an electric field value between 0 to 800 kV/m because the electrodes gap is 12.5 mm. For the calculation, we neglect the thickness of the glass wall which leads us to an uncertainty of 5% on the measurement. The SEF was applied for a period of 120 seconds. The experimental set up generates automatically the drop (about 5 seconds) and then the recording of surface tension starts. We observed that 120 seconds was enough to reach an equilibrium state for protein dynamic in the 8µL droplet. At the end of this time, a photo of the droplet was taken in each case, with or without SEF. Between each voltage value, a photo of the droplet was taken at 0 kV. The experiment was repeated 5 times for each solution and each voltage value. Then, the pictures of the droplets were transferred to the ImageJ software in order to calculate the ST according to the method presented in the following paragraph.

In an ideal equilibrium situation (no liquid withdrawal, zero flow rate), the tangential electric field on the electrified meniscus surface is zero. In the liquid side, the electric field vanishes, since there are no liquid motions and no need for a compensating electric field (Gañán-Calvo, Dávila, and Barrero 1997).

When the droplet is placed between two flat electrodes, the situation is a bit more complex. The distribution of electric charges is heterogeneous in the droplet, but is organized symmetrically on either side of the droplet center. The electrical relaxation time $t_e = \beta\varepsilon_0/K$ is small compared to the hydrodynamic time $T_h \sim L/U$, which is the time required for the fluid particles with characteristic velocity U to move across a zone of characteristic size L.

In that case, the liquid bulk is quasi-neutral and the free charges are confined to a very thin layer, of the order of Debye's length, underneath the liquid-gas interface (Nath, Borthakur, and Biswas 2020).

From the electrical point of view, the liquid bulk acts as an Ohmic conductor whose electric conductivity is given by the mobilities of the positive and negative ion species in a quasi neutral solution (Gañán-Calvo, Dávila, and Barrero 1997).

2.3 Apparent surface tension calculation method

Among different methods used for the measurement of interfacial tension, the pendant droplet is particularly well adapted to a liquid – liquid interface (Faour et al. 1996; Gassin 2014). It is based on the deformation of a droplet depending on the interfacial tension. To describe the

shape of interfaces (Figure 2), Young-Laplace introduced an equation that combines the curvature of the interface, the ST, and the hydrostatic pressure:

$$-\Delta\rho g z + \gamma\frac{2}{R_0} = \gamma\left[\frac{1}{r_1}+\frac{1}{r_2}\right] \quad (2)$$

The most usual method was developed by Rotenberg: from an approximated initial value of γ, Laplace's equation is numerically integrated by successive iterations using the Runge–Kutta method until the computed and the digitized profiles coincide (Berry et al. 2015). Using the dimensionless coordinates X, Y and S such as $X = \frac{x}{R_0}$, $Y = \frac{\gamma}{R_0}$, $S = \frac{s}{R_0}$ and using that $R_1 = \frac{ds}{d\theta}$ and $R_2 = \frac{x}{sin\theta}$ the Young-Laplace equation can be rewritten in the following parametric form (Dingle et al. 2005):

$$\frac{d\theta}{dS} = 2 - \beta Y - \frac{sin\theta}{X} \quad (3)$$

$$\frac{dX}{dS} = cos\theta$$

$$\frac{dY}{dS} = sin\theta \quad (4)$$

Here we define $\beta = \frac{\Delta\rho g {R_0}^2}{\gamma}$

To characterize the shape of the droplet, the parameter $\sigma = \frac{D_e}{D_s}$ was introduced. The use of the following polynomial formulas, which are approximations of the Fordham tables, allow to deduce from σ an approximate value of the two parameters β and R_0:

$$\beta = 0.12836 - 0.7577\sigma + 1.7713\sigma^2 - 0.5426\sigma^3 \quad (5)$$

$$\frac{D_e}{2R_0} = 0.9987 + 0.1987\beta - 0.0734\beta^2 + 0.34708\beta^3 \quad (6)$$

Thus, the value of the apparent ST was obtained as follows:

$$\gamma = \frac{\Delta\rho g {R_0}^2}{\beta} \quad (7)$$

As the ST is determined from experimental profiles of a droplet, it is considered as an apparent interfacial tension (Berry, 2015). The literature (Gassin, 2014) states that the results obtained with this method are an approximate value at about 10%. This uncertainty comes mainly from the uncertainties on β and R_0 related to their determination, and to the definition of the droplet

profile. More precise methods can be used but they require the numerical solution of Maxwell's equations and a huge computational effort (Dingle et al. 2005).

Several authors have been interested in measuring the ST of water as well as WPI and chickpea aquafaba solutions. They used the pendant drop tensiometer method coupled with image analysis, and the method that correlates ST to the drop time curves (Ghribi et al. 2015). Table 1 summarizes the different values of the ST of these solutions in the absence of an SEF. As expected, these data indicate that WPI and CKP considerably reduce the ST. These values are considered as reference measurements that should validate our methodology.

Berry et al. (2015) recall that the Young-Laplace equation can only be solved analytically for the trivial case where the drop profile is a sphere. As soon as the drop undergoes a geometrical deformation, the use of the Young-Laplace equation becomes more uncertain, and the equations must be solved numerically. The use of the Bond number is recommended to confirm the observations made by measuring the ST. The Bond number (Bo) is a dimensionless number that represents the ratio between the gravitational forces and the ST on an interface between two fluids:

$$Bo = \frac{\Delta\rho g {R_0}^2}{\gamma} \quad (8)$$

With:

- $\Delta\rho$, density difference of the two fluids (kg/m^3)
- R_0, characteristic length, here the radius of the drop (m) from its centre (initially defined when it had a spherical shape) to its edge

3. RESULTS

Figure 3 presents the influence of the SEF on the shape of distilled water, WPI and CKP solutions droplets generated with the pendant droplet tensiometer.

In order to verify that the changes in the geometry of the droplets observed in Figure 3 are reversible, we recorded an image 10 seconds after the SEF was stopped (Figure 4). With the example of the CKP, we can see that the droplet returns to its initial shape (i.e. the one it has when the SEF is not applied).

Figure 5 shows the evolution of the surface tension (calculated using the images, some of which are shown in Figure 4) as a function of the applied electric field.

3.1. Impact of SEF on distilled water droplets

When no voltage was applied across the electrodes, a spherical (Laplacian) droplet was observed. As the voltage increased, the droplet elongated in the direction of the gravitational field, in a direction perpendicular to the applied SEF. Siedel et al. (2018) noted an elongation of the droplets in the same direction as the electrostatic force, but their experimental set-up was different (electrodes positioned at the top and bottom, not at the side, and generation of gas bubbles, not liquid). The fact that the droplets exposed deformation perpendicularly to the applied SEF can be explained by the reduction of the ST at the air/liquid interface (Sato, Kudo, and Saito 1999): the cohesive forces that interact within the droplet allowing it to maintain its spherical shape were reduced, the droplet was then more subjected to the gravitational field, and it deformed in the same direction as that field. As mentioned by Filali, Er-Riani, and El Jarroudi (2021), the electric field discontinuity across the interface creates a jump of Maxwell's stress tensor that is similar to an electric pressure. The cohesive forces were so reduced when high voltages (10 kV) were applied that it became difficult to generate a single droplet at the tip of the syringe; as a consequence, the droplets detached from the syringe on some occasions.

3.2. Impact of SEF on WPI solution droplet

For WPI and CKP aquafaba solutions, the observations and deductions were similar to those made with the previous case (distilled water). However, it should be noted that the droplet deformed more at lower voltages than in the distilled water case. This can be explained by a cumulative effect due to the presence of the WPI: the proteins have their own surface active effect (Said et al. 2022), which reduced the ST and came in synergy to the effect of the electrostatic field. It was not possible to take pictures of droplets at 8 and 10 kV because the surface voltage was too low to generate a droplet at the tip of the syringe. Either the droplet remained too short before it broke off to make a clear picture, or a continuous stream of liquid escaped from the needle.

3.3. Impact of SEF on chickpea aquafaba droplets

It was not possible to obtain images at 8 or 10kV for the same reasons as explained above. The same effects of SEF on the CKP droplet as with the WPI droplet were observed: elongation in the direction of the gravitational field, droplet deformed more at lower voltages than in the distilled water case. According to Figure 5, the ST values for each applied voltage were close between WPI and CKP, WPI being slightly more surface active than CKP at 0kV. This is in

line with the literature (Oo and Soe 2017) which proposes CKP as a vegetable alternative to WPI.

3.4. Impact of SEF on the apparent surface tension

The Figure 5 shows the evolution of the ST at the air/liquid interface of the droplet as a function of the electric field strength (applied voltage on the electrode gap). A clear decrease in apparent ST was observed with increasing voltage: 68% for distilled water, 54% for WPI and 53% for CKP (values for a decrease in ST between 0 and 6 kV). A similar protein content (about 3%) may explain the very similar evolution between WPI and CKP. The slight differences observed can be explained by the structural differences of the WPI and CKP proteins.

These observations are supported by the evolution of the Bond number as a function of the applied electric field (Figure 7). We observe a decrease of the Bond number with the increase of the voltage applied to the terminals of the electrodes. Bo being defined as the ratio between the gravitational forces and the ST, we can therefore confirm that the ST decreases. Berry et al. (2015) consider that the pendant droplet tensiometry is a simple method to determine the interfacial tension, but they warn that the method is inaccurate when the Bond number is low. They consider that the method is no longer suitable if $Bo<0.1$, which is not our case.

In distilled water, molecules undergo very short-range interactions (attractive Van der Waals interaction). The Van der Waals bond is the electrostatic attraction or repulsion between molecules with permanent or temporary dipoles. The application of the electric field changes the dipole moment of the water molecules, which also changes the anisotropy of the molecular interaction forces, thus decreasing the ST.

For solutions containing proteins, this effect is present but the effect of the electric field on the proteins is also added.

The surface-active properties of proteins are due to their amphiphilic structure, which prevents the immediate recombination of newly created droplets via the Marangoni effect, stabilizes the formed droplets by decreasing the pressure gradient at the interface, and stabilizes the droplets against aggregation, by providing electrostatic or steric repulsions between the droplets.

As the function of proteins depends directly on their structure, any constraint imposed by the presence of an electric field can potentially become harmful. Astrakas, Gousias, and Tzaphlidou (2011) have shown that the electric field induces conformational changes in proteins. In addition, there is evidence that the electric field accelerates the folding and unfolding rates of

globular proteins in solution. For example, exposure to electric and electromagnetic fields may be considered in the design of alternative treatment strategies for amyloid diseases because of their inhibitory effect on the conformations of amyloid gene peptides of intermediate strength (De Pomerai et al. 2003). Some studies on the alterations of protein conformations under the influence of SEF, show the role of hydrogen bonds. Hydrogen bonds play a fundamental role in controlling protein activity during enzymatic action─folding, binding with other proteins, and other processes. Changes in the strength of hydrogen bonds, induced by an electric field, can affect these processes (Astrakas, Gousias, and Tzaphlidou 2011).

Sato et al. (1999) calculated that the ST reduction due to applied voltage was proportional to the square of the voltage. We also introduce a quantity γ_E, called ST reduction, which is calculated as follows:

$$\gamma_E = \gamma_0 - \gamma \tag{9}$$

With:

- γ_0, value of surface tension when no voltage was applied
- γ, value of surface tension at a single value of applied voltage

The ST reduction (defined by equation 9) as a function of the voltage applied is plotted in Figure 6. As shown in the figure, the model proposed by Sato was not adequate in our case where a power law is suited. This difference is due to the measurement method used by Sato et al.. They proposed a specific equation to calculate the ST from the theory on vibrating but it required some correction factors. As previously explained, our calculation method is based on the traditional Young-Laplace equation, which applies to spherical drops. Bateni, Amirfazli, and Neumann (2006) performed an error analysis to examine the quality of the Laplacian curve fittings at high voltages. It was found that the measurements between 1kV to 7 kV are generally at the same level of reliability as those in the absence of an electric field. The measurements up to 8 kV were found to be less reliable, possibly because the shape of a drop deviates from the Laplacian relation, close to the stability limit.

According to Mhatre et al. (2019), the classically used Young-Laplace equation could be modified to include electrostatic effects. When a drop is exposed to an electric field, the shape of the drop at equilibrium is due to the Maxwell stress at its interface which is balanced by an interfacial tension force. Starting from the equation (2), they define the modified Young-Laplace equation in SEF:

$$\gamma\left(\frac{1}{R_1}+\frac{1}{R_2}\right)=\Delta\rho_0-\Delta\rho gz+\frac{1}{2}\in.E_n^2 \quad (10)$$

Where:

- $\in$ is permittivity of the medium phase
- E_n is the normal component of SEF at the drop interface
- The last term on the right side of the above equation denotes the normal component of the Maxwell stress.

This additional term is suited for a perfectly conducting drop in a pure dieletric medium. Mhatre et al. (2019) indicated that as the strength of the SEF increases, the radius of curvature at the top of the drop decreases, but if the Maxwell stress term is not included in the Young-Laplace equation, the estimated interfacial tension is misleading and significantly lower than the real interfacial tension. A further step will consist in developing a specific new algorithm to evaluate the ST from Eq. 10.

4. CONCLUSION & PERSPECTIVES

The pioneer investigations presented in this paper aimed at assessing the impact of an external SEF on the apparent ST of 3 model solutions. It was confirmed that applying an SEF yielded a significant reduction of the ST of water. Two aqueous protein solutions have been considered too, also resulting in a significant reduction of the ST under SEF (up to 48%).

This decrease in ST can be explained by:

- A modification of the dipole moments between molecules
- A modification of the H-bonds and Van der Waltls type interactions
- A change in the conformation of proteins, which then lose their structural properties

If the shape of the drop is clearly altered by the SEF, other data treatments should be performed using the modified Young-Laplace equation. In the search for an innovative process to stabilise food foams, SEF treatment appears therefore as a promising solution. By reducing the ST, liquid or gas droplets exposed to SEF are likely to break up more easily under shearing conditions. Food protein matrices, such as food foams, are even more sensitive to the effect of SEF because they contain proteins that already have a surfactant effect. By facilitating expansion through the

formation of small gas bubbles, SEF reduces the energy consumption required to operate a mixer and limits the use of surface-active chemicals traditionally used to lower the ST and stabilise the foam over time. Thus, expansion coupled with SEF offers new horizons in terms of processing using "clean labelled" foams or emulsions.

ACKNOWLEDGEMENTS

The present paper/communication has been co–funded by ONIRIS-GEPEA and by the FEDER European funds Ref 2020/FEDER/n°PL0019794 within the international Chair "CONT-E-FOOD" on continuous food processes under electrical disturbances. Disclaimer: the content found in this contribution reflects only the author's view. The EU commission is not responsible for any use that may be made of the information it contains.

We thank Pedro Llovera-Segovia (Instituto de Tecnología Electrica - Universitat Politecnica de Valencia, Spain) for his contribution on electrostatic phenomena.

REFERENCES

Astrakas, Loukas, Christos Gousias, and Margaret Tzaphlidou. 2011. "Electric Field Effects on Chignolin Conformation." *Journal of Applied Physics* 109 (9). https://doi.org/10.1063/1.3585867.

Audebert, Alexia. 2018. "Stabilisation et Texturation de Mousses Liquides Par Des Protéines de Lactosérum Chauffées à l'état de Poudre." Université Bretagne Loire. https://www.theses.fr/2018NSARB317.

Bateni, A., A. Amirfazli, and A. W. Neumann. 2006. "Effects of an Electric Field on the Surface Tension of Conducting Drops." *Colloids and Surfaces A: Physicochemical and Engineering Aspects* 289 (1–3): 25–38. https://doi.org/10.1016/j.colsurfa.2006.04.016.

Bazinet, Laurent, Maher Trigui, and Denis Ippersiel. 2004. "Rheological Behavior of WPI Dispersion as a Function of PH and Protein Concentration." *Journal of Agricultural and Food Chemistry* 52 (17): 5366–71. https://doi.org/10.1021/jf049893v.

Berry, Joseph D., Michael J. Neeson, Raymond R. Dagastine, Derek Y.C. Chan, and Rico F. Tabor. 2015. "Measurement of Surface and Interfacial Tension Using Pendant Drop Tensiometry." *Journal of Colloid and Interface Science* 454: 226–37. https://doi.org/10.1016/j.jcis.2015.05.012.

Boissonnet, Guillaume. 1998. "Étude de l'écoulement d'une Mousse Aqueuse de

Décontamination Hydrodynamique." Université de Montpellier II.

Bonhomme, Oriane, Li Peng, and Anne Laure Biance. 2020. "Thermally Enhanced Electro-Osmosis to Control Foam Stability." *Physical Review X* 10 (2). https://doi.org/10.1103/PhysRevX.10.021015.

Borthakur, Manash Pratim, Gautam Biswas, and Dipankar Bandyopadhyay. 2018. "Dynamics of Drop Formation from Submerged Orifices under the Influence of Electric Field." *Physics of Fluids* 30 (12). https://doi.org/10.1063/1.5063913.

Castellanos, Antonio. 1998. "Electrospray and Atomization." In *Electrohydrodynamics*, 206–12. Vienna: Springer Vienna. https://doi.org/10.1007/978-3-7091-2522-9_14.

Dingle, Nicole M., Kristianto Tjiptowidjojo, Osman A. Basaran, and Michael T. Harris. 2005. "A Finite Element Based Algorithm for Determining Interfacial Tension (γ) from Pendant Drop Profiles." *Journal of Colloid and Interface Science* 286 (2): 647–60. https://doi.org/10.1016/j.jcis.2005.01.052.

Faour, G, M Grimaldi, J Richou, and A Bois. 1996. "Real-Time Pendant Drop Tensiometer Using Image Processing with Interfacial Area and Interfacial Tension Control Capabilities." *Journal of Colloid and Interface Science* 181 (2): 385–92. https://doi.org/10.1006/jcis.1996.0395.

Felix, Manuel, Inmaculada Martínez, Ana Sayago, and Mª Ángeles Fernández Recamales. 2021. "Wine Lees: From Waste to O/W Emulsion Stabilizer." *Innovative Food Science and Emerging Technologies* 74 (August). https://doi.org/10.1016/j.ifset.2021.102810.

Filali, Youness, Mustapha Er-Riani, and Mustapha El Jarroudi. 2021. "Deformation of a Fluid Drop Subjected to a Uniform Electric Field." *Zeitschrift Fur Angewandte Mathematik Und Physik* 72 (1): 1–18. https://doi.org/10.1007/s00033-020-01439-w.

Gañán-Calvo, A. M., J. Dávila, and A. Barrero. 1997. "Current and Droplet Size in the Electrospraying of Liquids. Scaling Laws." *Journal of Aerosol Science* 28 (2): 249–75. https://doi.org/10.1016/S0021-8502(96)00433-8.

Gassin, Pierre-Marie. 2014. "Mesure de La Tension Superficielle Par La Technique de La Goutte Pendante." https://www.researchgate.net/publication/260963141.

Ghribi, Abir Mokni, Ines Maklouf Gafsi, Christophe Blecker, Sabine Danthine, Hamadi Attia, and Souhail Besbes. 2015. "Effect of Drying Methods on Physico-Chemical and

Functional Properties of Chickpea Protein Concentrates." *Journal of Food Engineering* 165: 179–88. https://doi.org/10.1016/j.jfoodeng.2015.06.021.

Kovalchuk, N., F. Alberini, and M. J.H. Simmons. 2020. "Effect of Moderate DC Electric Field on Formation of Surfactant-Laden Drops." *Chemical Engineering Research and Design* 157 (6): 133–41. https://doi.org/10.1016/j.cherd.2020.03.009.

Liu, Jianshu, and Yang Cao. 2021. "Experimental Study on the Surface Tension of Magnetized Water." *International Communications in Heat and Mass Transfer* 121 (December 2020): 105091. https://doi.org/10.1016/j.icheatmasstransfer.2020.105091.

Mhatre, Sameer, Sébastien Simon, and Johan Sjöblom. 2019. "Methodology to Calculate Interfacial Tension under Electric Field Using Pendent Drop Profile Analysis." *Proceedings of the Royal Society A: Mathematical, Physical and Engineering Sciences* 475 (2225). https://doi.org/10.1098/rspa.2018.0852.

Nath, Binita, Manash Pratim Borthakur, and Gautam Biswas. 2020. "Electric Field Induced Dynamics of Viscoplastic Droplets in Shear Flow." *Physics of Fluids* 32 (9). https://doi.org/10.1063/5.0021829.

Nicorescu, Irina. 2009. "Étude Du Couplage Procédé/Produit Lors De La Production Des Mousses Par Des Agrégats Protéiques." Nantes Université. https://tel.archives-ouvertes.fr/tel-00872696/document.

Notz, Patrick K., and Osman A. Basaran. 1999. "Dynamics of Drop Formation in an Electric Field." *Journal of Colloid and Interface Science* 213 (1): 218–37. https://doi.org/10.1006/jcis.1999.6136.

Oo, Zar, and Soe Soe. 2017. "Physico Chemical and Functional Properties of Chickpea Protein Isolate." *International Journal of Biological & Pharmaceutical Research* 3 (12): 1–14.

Pomerai, David I. De, Brette Smith, Adam Dawe, Kate North, Tim Smith, David B. Archer, Ian R. Duce, Donald Jones, and E. Peter M. Candido. 2003. "Microwave Radiation Can Alter Protein Conformation without Bulk Heating." *FEBS Letters* 543 (1–3): 93–97. https://doi.org/10.1016/S0014-5793(03)00413-7.

Rio, Emmanuelle. 2013. "Stabilité Des Mousses : Quelques Expériences Montrant l'influence de La Rhéologie de Surface." https://tel.archives-ouvertes.fr/tel-00874063.

Said, Mohamed Sasi, Mohd Zaidi Jaafar, Shaziera Omar, and Sairoz Norazlan Sharbini. 2022.

"Influence of Whey Protein Isolate on CO2 Foams Stability in Three Different Types of Crude Oil." *Case Studies in Chemical and Environmental Engineering* 5 (May). https://doi.org/10.1016/j.cscee.2022.100191.

Sato, Masayuki, Naoya Kudo, and Masahiro Saito. 1999. "Surface Tension Reduction of Liquid by Applied Electric Field Using Vibrating Jet Method." *IEEE Transactions on Industry Applications*.

Schramm, Laurier L. 2006. *Emulsions, Foams and Suspensions*. *Emulsions, Foams, and Suspensions*. Wiley-VCH Verlag GmbH & Co. KGaA. https://doi.org/10.1002/3527606750.fmatter.

Siedel, Samuel. 2012. "Bubble Dynamics and Boiling Heat Transfer: A Study in the Absence and in the Presence of Electric Field." *Ph.D. Thesis, Institut National De Sciences Appliquees De Lyon*. http://theses.insa-lyon.fr/publication/2012ISAL0032/these.pdf.

Wang, Junjing, Morane Jousse, Jitesh Jayakumar, Alejandro Fernández-Arteaga, Silvia de Lamo-Castellví, Montserrat Ferrando, and Carme Güell. 2021. "Black Soldier Fly (Hermetia Illucens) Protein Concentrates as a Sustainable Source to Stabilize o/w Emulsions Produced by a Low-Energy High-Throughput Emulsification Technology." *Foods* 10 (5). https://doi.org/10.3390/foods10051048.

Yousif, Adel M., Richard Snowball, Mario F. D'Antuono, Harmohinder S. Dhammu, and Darshan L. Sharma. 2021. "Water Droplet Surface Tension Method – An Innovation in Quantifying Saponin Content in Quinoa Seed." *Food Chemistry* 343 (May 2020): 128483. https://doi.org/10.1016/j.foodchem.2020.128483.

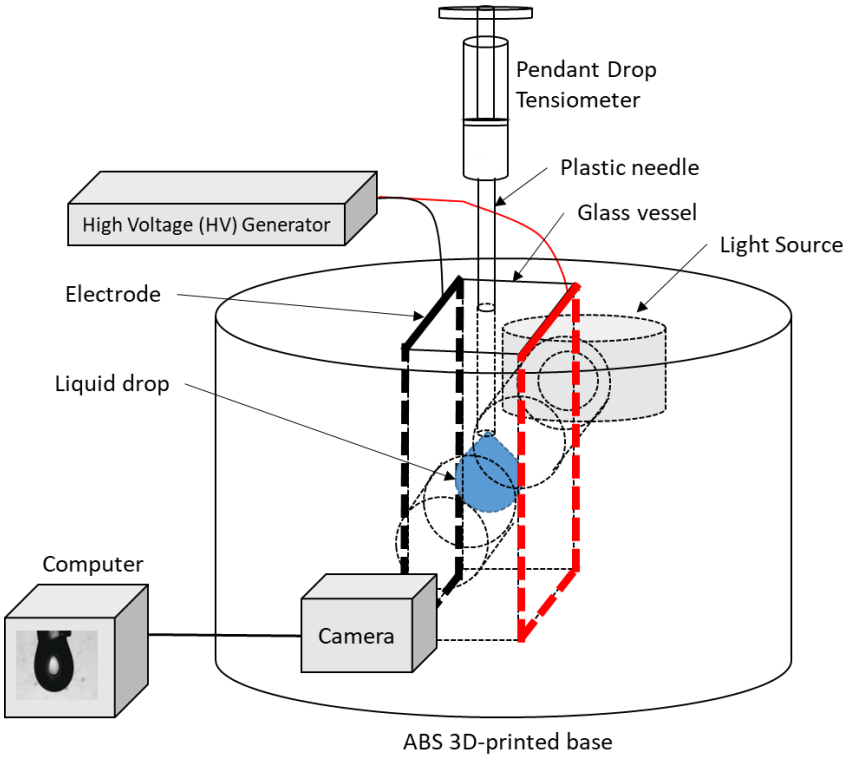

Figure 1 : Pendant droplet tensiometer modified with two parallel electrodes to generate static electric field

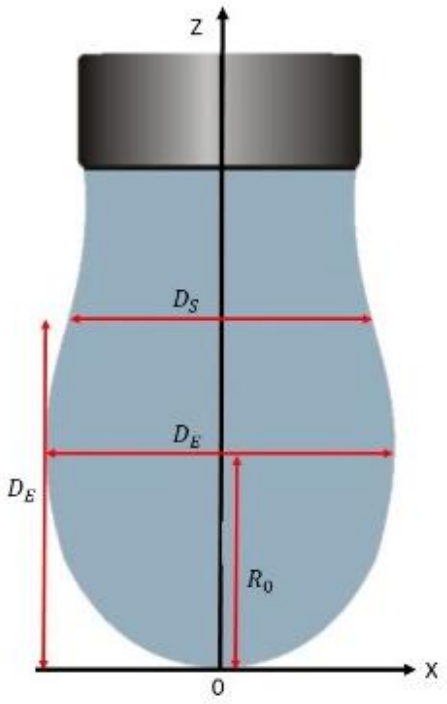

Figure 2 : Schema of a pendant droplet with its main geometric dimensions necessary for image analysis

Table 1 : Distilled water, 3% WPI solution and Chickpea aquafaba surface tension values at 0kV found in the literature

References	Surface tension values at 0kV		
	Distilled water	*WPI (3%)*	*CKP (3%)*
Sato et al., 1996	72.28		
Yousif et al., 2020	72.15		
Yadav et al., 2020	72		
Xu et al., 2013		49	
Adhikari et al., 2006		42.5	
Ghribi et al., 2015			42

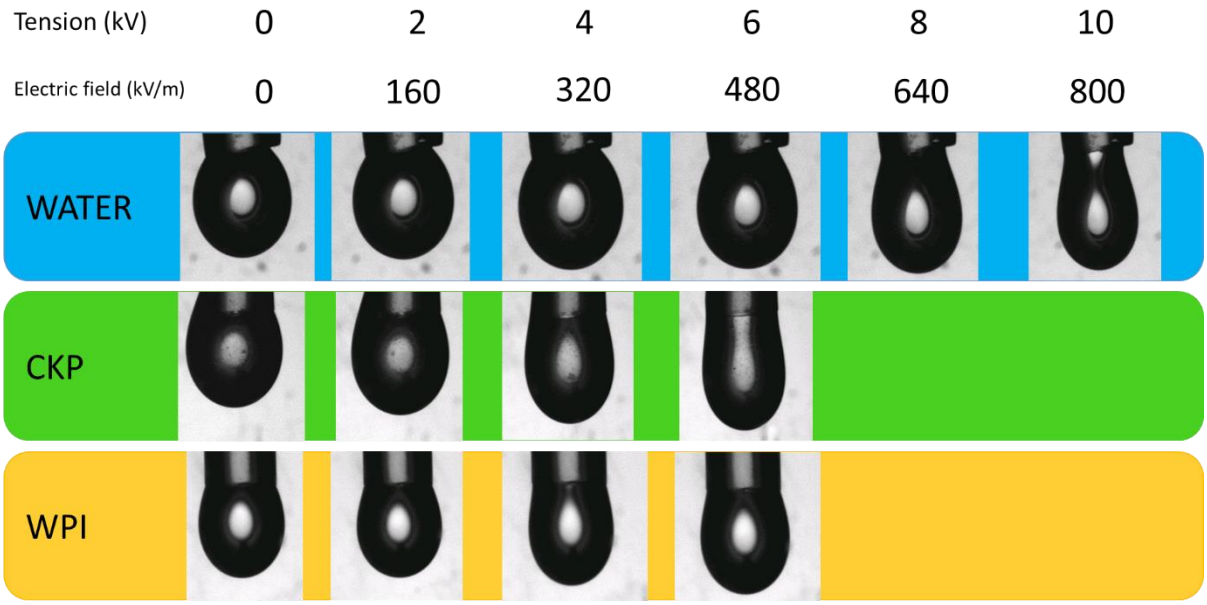

Figure 3 : Photos of pendant droplets deformed when an electric field is applied at different voltage values

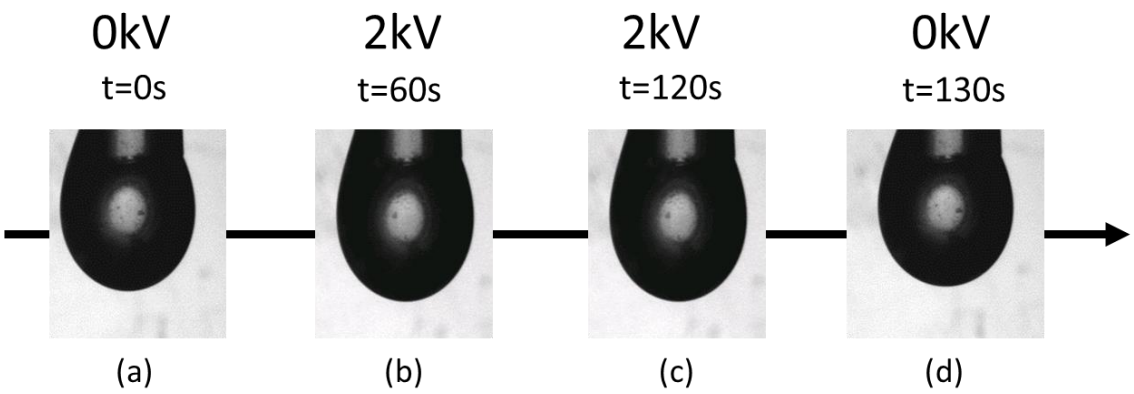

Figure 4 : Photos of CKP pendant droplets during an experiment. (a) Beginning of the experiment (b) Picture at middle of the experiment (c) Photo at the end of the experiment (d) Photo 10s after the end of the experiment

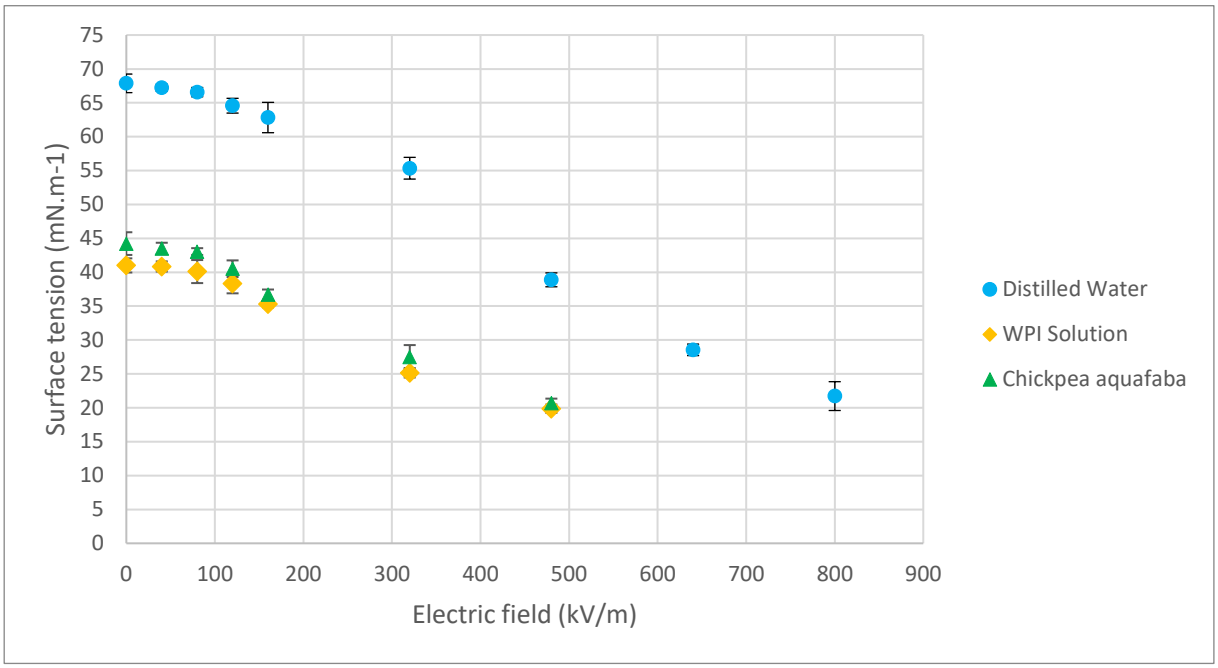

Figure 5 : Evolution of the surface tension as a function of the electric field applied to the electrodes

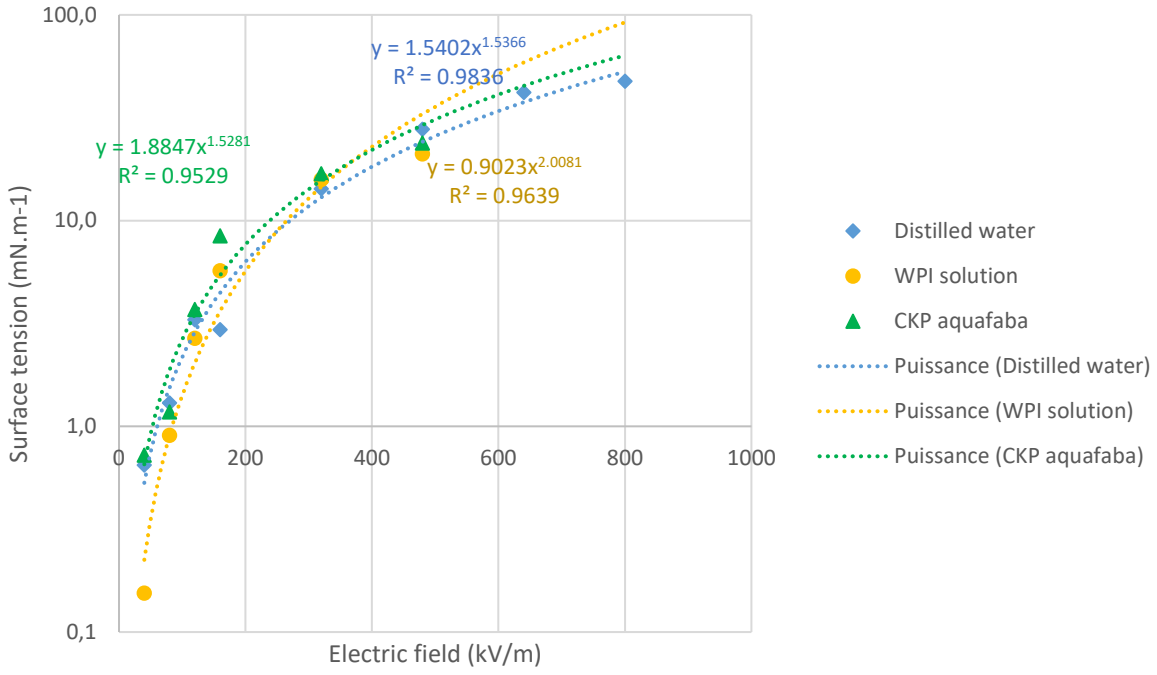

Figure 6: Surface tension reduction as a function of the electric field applied to the electrode on each side of the pendant drop

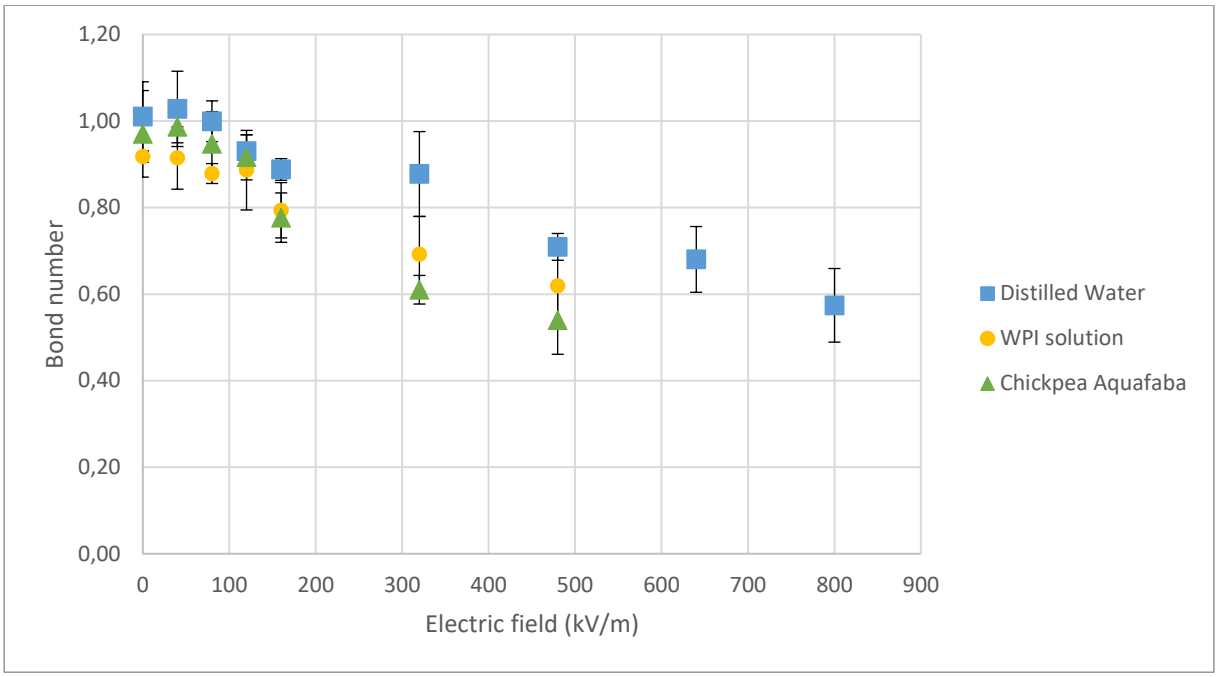

493

494 *Figure 7: Evolution of the Bond number as a function of the electric field applied to the electrodes*

495